HHS Public Access

Author manuscript

Nat Neurosci. Author manuscript; available in PMC 2016 February 01.

Published in final edited form as:

Nat Neurosci. 2015 April ; 18(4): 521–530. doi:10.1038/nn.3966.

GLUT1 reductions exacerbate Alzheimer's disease vasculoneuronal dysfunction and degeneration

Ethan A. Winkler[#1,2], **Yoichiro Nishida**[#3,4], **Abhay P. Sagare**[#1], **Sanket V. Rege**[1], **Robert D. Bell**[3], **David Perlmutter**[3], **Jesse D. Sengillo**[1,3], **Sara Hillman**[3], **Pan Kong**[1], **Amy R. Nelson**[1], **John S. Sullivan**[1], **Zhen Zhao**[1], **Herbert J. Meiselman**[5], **Rosalinda B. Wendy**[5], **Jamie Soto**[6], **E. Dale Abel**[6], **Jacob Makshanoff**[1], **Edward Zuniga**[1], **Darryl C. De Vivo**[7], and **Berislav V. Zlokovic**[1,5,§]

[1] Zilkha Neurogenetic Institute, Keck School of Medicine, University of Southern California, Los Angeles, CA

[2]Department of Neurological Surgery, University of California San Francisco, San Francisco, CA

[3] Center for Neurodegenerative and Vascular Brain Disorders, University of Rochester School of Medicine & Dentistry, Rochester, NY

[4]Department of Neurology and Neurological Science, Graduate School, Tokyo Medical and Dental University, Tokyo, Japan

[5]Departrment of Physiology and Biophysics, Keck School of Medicine, University of Southern California, Los Angeles, CA

[6]Fraternal Order of Eagles Diabetes Research Center and Division of Endocrinology and Metabolism, Carver College of Medicine, University of Iowa, Iowa City, IA, USA

[7]Colleen Giblin Laboratories for Pediatric Neurology Research, Columbia University New York, NY, USA

[#] These authors contributed equally to this work.

Abstract

The glucose transporter GLUT1 at the blood-brain barrier (BBB) mediates glucose transport into the brain. Alzheimer's disease is characterized by early reductions in glucose transport associated with diminished GLUT1 expression at the BBB. Whether GLUT1 reduction influences disease pathogenesis remains, however, elusive. Here, we show that GLUT1 deficiency in mice overexpressing amyloid β-petpide (Aβ) precursor protein leads to: 1) early cerebral microvascular

[§]corresponding author, Berislav V. Zlokovic, M.D., Ph.D., Zilkha Neurogenetic Institute, 1501 San Pablo Street, Los Angeles, CA 90089, Phone: 323.442.2722 / Fax: 323.666.2184, zlokovic@usc.edu.

Authors' contribution: E.A.W. contributed to manuscript preparation, experimental design/analysis and conducted experiments. Y.N. and A.P.S. contributed to experimental design, data analysis and interpretation, and conducted experiments. S.R., R.D.B., J.D.S., S.H., J.S.S., P.K., A.R.N., R.B.V., J.M., E.Z. and Z.Z. conducted and analyzed experiments. H.J.M. contributed to hematological analysis and data interpretation. E.D.A. provided *Slc2a1*$^{lox/lox}$ mice and contributed to project design. J.S. generated *Slc2a1*$^{lox/+}$*Tie2-Cre* mice. D.C.D. provided *Slc2a1*$^{+/-}$ mice and contributed to project design. B.V.Z. supervised and designed all experiments and analysis and wrote the manuscript.

Conflict of Interest

None of the authors has conflict of interest.

degeneration, blood flow reductions and dysregulation, and BBB breakdown; and (2) accelerated amyloid β-peptide (Aβ) pathology, reduced Aβ clearance, diminished neuronal activity, behavioral deficits, and progressive neuronal loss and neurodegeneration that develop after initial cerebrovascular degenerative changes. We also show that GLUT1 deficiency in endothelium, but not in astrocytes, initiates the vascular phenotype as shown by BBB breakdown. Thus, reduced BBB GLUT1 expression worsens Alzheimer's disease cerebrovascular degeneration, neuropathology and cognitive function suggesting that GLUT1 may represent a novel therapeutic target for Alzheimer's disease vasculo-neuronal dysfunction and degeneration.

Introduction

The glucose transporter GLUT1, encoded by *SLC2A1*, mediates glucose transport into the brain[1, 2]. GLUT1 is expressed at the blood-brain barrier (BBB), but not in neurons[1, 2]. GLUT1 exists in two isoforms – a 55 kDa isoform in brain endothelial cells and a 45 kDa isoform in adjacent astrocyte end-foot processes[3]. The crystal structure of human GLUT1 has been recently reported[4]. Brain glucose uptake correlates with GLUT1 levels in cerebral microvessels[5-7]. GLUT1 deficiency is found in patients with epilepsy, movement disorders and cognitive impairment[8]. In mice, GLUT1 haploinsufficiency (*Slc2a1*$^{+/-}$) diminishes glucose cerebrospinal fluid (CSF) levels and leads to microencephaly[9, 10]. In the zebrafish, GLUT1 is required for the formation of the BBB[11], raising a possibility for its dual role similar to twofold role of the major facilitator family domain containing 2a (MFSD2A) transporter, which transports essential fatty acids across the BBB into the brain and regulates BBB integrity[12-14].

Dementia due to Alzheimer's disease (AD) is characterized by progressive metabolic disturbances[15], neurovascular dysfuction[1, 2] and BBB breakdown[16]. Diminished glucose uptake in the hippocampus, parietotemporal cortex and/or posterior cingulate cortex in individuals at genetic risk for AD[17,18], positive family history[19], and/or mild or no cognitive impairment who develop AD[20, 21] has been shown by 2-[^{18}F] fluoro-2-deoxy-D-glucose positron emission tomography (FDG-PET). FDG-PET changes precede brain atrophy and neuronal dysfunction in humans[18, 22] and transgenic AD models[23], which may reflect reductions in BBB glucose transport[24,25]. Reduced GLUT1 levels in cerebral microvessels were also found in AD[26-29]. Whether GLUT1 reductions can lead to cerebrovascular damage contributing to and/or accelerating AD-like neurodegeneration remains, however, elusive.

To address this question, we crossed transgenic mice overexpressing human amyloid β-peptide (Aβ) precursor protein (*APP*$^{Sw/0}$)[30] with GLUT1-deficient *Slc2a1*$^{+/-}$ mice[9]. We also utilized conditional *Slc2a1* $^{lox/lox}$ mice[31] to determine the effects of cell-specific GLUT1 deletions from endothelium and astrocytes on the BBB phenotype. We show that GLUT1 is necessary for the maintenance of proper brain angioarchitecture, cerebral blood flow (CBF) and BBB integrity, and that GLUT1 reductions in *APP*$^{Sw/0}$ mice accelerate Aβ accumulation and lead to progressive neuronal dysfunction, behavioral deficits, neuronal loss and neurodegeneration that develop after initial cerebrovascular changes. We also show that GLUT1 deficiency in endothelium, but not in astrocytes, initiates the BBB breakdown. Our

data suggest that GLUT1 reductions at the BBB play an early pathogenic role in neuronal demise in an AD-like neurodegenerative process.

Results

Microvascular reductions and diminished cerebral blood flow and glucose uptake in GLUT1-deficient *APP$^{Sw/0}$* mice

Immunofluorescent staining for endothelial-specific *Lycopersicon esculentum* lectin and GLUT1 (**Supplementary Fig 1a-b**) and immunoblotting of brain microvessels (**Supplementary Fig 1c-d**), show ~50% reduction in GLUT1 brain endothelial levels in 6 month-old *Slc2a1$^{+/-}$* and *Slc2a1$^{+/-}$APP$^{Sw/0}$* mice compared to their respective age-matched littermate controls (**Supplementary Fig 1a-d**). There was no difference in GLUT1 levels between *Slc2a1$^{+/+}$APP$^{Sw/0}$* and *Slc2a1$^{+/+}$* mice and/or *Slc2a1$^{+/-}$APP$^{Sw/0}$* and *Slc2a1$^{+/-}$* mice (**Supplementary Fig 1a-d**).

No alterations in blood glucose were detected in *Slc2a1$^{+/+}$, Slc2a1$^{+/-}$*, *Slc2a1$^{+/+}$APP$^{Sw/0}$* or *Slc2a1$^{+/-}$APP$^{Sw/0}$* mice (**Supplementary Fig 1e**). In contrast, significant 57% and 70% reductions in CSF glucose levels and the CSF-to-blood glucose ratios were found in 6-month-old *Slc2a1$^{+/-}$* and *Slc2a1$^{+/-}$APP$^{Sw/0}$* mice compared to *Slc2a1$^{+/+}$* littermates (**Supplementary Fig 1e-f**). CSF glucose levels were also reduced by ~25% in *APP$^{Sw/0}$* mice despite unaltered GLUT1 BBB levels. Notably, microvascular and CBF reductions, as found in early disease stage in *APP* lines[32-34] (see **Fig 1** below), can both diminish glucose brain uptake independently of GLUT1 expression by reducing the capillary surface area available for glucose transport and the flow-dependent delivery of glucose to the brain[1, 2], respectively.

To evaluate whether reduced BBB GLUT1 expression affects brain microvascular structure, we analyzed the length of capillary networks using lectin-positive profiles (as in **Supplementary Fig 1a**). We found significant 21% and 16% reductions in capillary length in 2 week-old *Slc2a1$^{+/-}$APP$^{Sw/0}$* mice in somatosensory cortex and hippocampus, respectively, when compared to other genotypes, which progress with age as shown by greater 37% and 33% and 54% and 49% reductions in capillary length in cortex and the CA1 hippocampal subfield in 1- and 6-month-old *Slc2a1$^{+/-}$APP$^{Sw/0}$* mice compared to *Slc2a1$^{+/+}$* littermate controls, respectively (**Fig 1a-b**). *Slc2a1$^{+/-}$* and *Slc2a1$^{+/+}$APP$^{Sw/0}$* mice displayed less pronounced microvascular reductions only at a later stage at 6 months of age (**Fig 1a-b**).

To find out whether brain capillary reductions determined by *ex vivo* histologic quantification reflect a perfusion deficit *in vivo,* we utilized *in vivo* multiphoton microscopy following injection of a fluorescein-conjugated dextran vascular tracer (MW: 70,000 Da) to generate 3D 0.5 mm Z stack cortical angiograms. Analysis of angiograms revealed 32%, 26% and 48% reductions in perfused cortical capillary length in 6-month-old *Slc2a1$^{+/-}$*, *Slc2a1$^{+/+}$APP$^{Sw/0}$* or *Slc2a1$^{+/-}$APP$^{Sw/0}$* mice compared to age-matched *Slc2a1$^{+/+}$* littermates, respectively (**Fig 1c-d**), suggesting that diminished BBB GLUT1 expression or *APP* overexpression is sufficient to reduce brain capillary density resulting in a perfusion

deficit, but when acting together they exert strong synergistic effect causing early loss of brain capillaries at 2 weeks of age as shown in *Slc2a1*$^{+/-}$*APP*$^{Sw/0}$ mice.

As regional brain capillary density closely correlates with regional CBF[1], we next evaluated whether brain capillary reductions lead to diminished resting CBF. ^{14}C-iodoantipyrine quantitative autoradiography revealed approximately 39% and 37% reductions in cortical and hippocampal blood flow in 1-month-old *Slc2a1*$^{+/-}$*APP*$^{Sw/0}$ mice, respectively, when compared to other genotypes (**Fig 1e-f**). *Slc2a1*$^{+/-}$ and *Slc2a1*$^{+/+}$*APP*$^{Sw/0}$ mice did not show reductions in cortical and hippocampal blood flow at 1 month of age. Within 6 months, however, both *Slc2a1*$^{+/-}$ and *Slc2a1*$^{+/+}$*APP*$^{Sw/0}$ mice developed significant 36% and 31% and 36% and 30% reductions in cortical and hippocampal blood flow that were less pronounced compared to 50% and 45% reductions found in *Slc2a1*$^{+/-}$*APP*$^{Sw/0}$ mice, respectively (**Fig 1e-f**). Hemodynamic and physiologic parameters which may influence CBF including mean arterial blood pressure, respiratory rate, heart rate, blood pH, arterial PCO_2 and arterial PO_2 did not significantly differ among *Slc2a1*$^{+/+}$, *Slc2a1*$^{+/-}$, *Slc2a1*$^{+/+}$*APP*$^{Sw/0}$ or *Slc2a1*$^{+/-}$*APP*$^{Sw/0}$ mice on the same mixed genetic background (**Supplementary Fig 2a-i**).

Laser Doppler flowmetry studying functional hyperemic responses to whisker-barrel vibrassal stimulation revealed early and significantly greater age-dependent reductions in CBF responses in 1 month old *Slc2a1*$^{+/-}$*APP*$^{Sw/0}$ mice compared to *Slc2a1*$^{+/-}$ and *Slc2a1*$^{+/+}$*APP*$^{Sw/0}$ mice that both develop less pronounced changes beginning at 6 months of age (**Fig 1g**). No changes in CBF responses were observed in *Slc2a1*$^{+/+}$ littermates. Collectively, these data show that both resting CBF and CBF responses are impaired early in animals with diminished GLUT1 function in the presence of the *APP* transgene, and are further worsened with age compared to either GLUT1-deficient mice or *APP* $^{Sw/0}$ mice alone.

The autoradiography analysis with 2[^{14}C]-deoxyglucose (2-DG) indicated diminished 2DG uptake by ~32-36% and 26-30% in the cortex and hippocampus (**Fig 1h**) and other brain regions (**Supplementary Table 1**) at an early stage in *Slc2a1*$^{+/-}$ and *Slc2a1*$^{+/-}$*APP*$^{Sw/0}$ mice suggesting that reduced glucose BBB transport leads to reduced brain glucose levels.

GLUT1 deficiency leads to early blood-brain barrier breakdown

GLUT1 reductions result in BBB breakdown in the developing zebrafish[11] and *in vitro* BBB models[35]. To examine whether similar relationship exists in the adult mammalian brain, we next sought to characterize BBB integrity through leakage of endogenous plasma proteins, such as fibrin and immunoglobulin G (IgG), in *Slc2a1*$^{+/-}$ mice. Young 2-week-old *Slc2a1*$^{+/-}$ mice demonstrated gross microvascular leakage and extravascular accumulation of circulating fibrin and immunoglobulin G (IgG) with 10-fold and 11-fold increases compared to control age-matched *Slc2a1*$^{+/+}$ littermates, respectively (**Fig 2a-c**). A much smaller but statistically significant 1.5 and 2-fold increase in extravascular fibrin and IgG was observed in 2-week-old *Slc2a1*$^{+/+}$*APP*$^{Sw/0}$ mice compared to age-matched *Slc2a1*$^{+/+}$ controls (**Fig 2a-c**) consistent with previous findings demonstrating early cerebral microvascular changes and BBB breakdown in *APP*$^{Sw/0}$ mice prior to significant Aβ

accumulation[36-38]. On the other hand, there was a substantial approximately 18- and 20-fold increase in parenchymal accumulates of plasma-derived fibrin and IgG in *Slc2a1*$^{+/-}$*APP*$^{Sw/0}$ mice, respectively, when compared to *Slc2a1*$^{+/+}$ littermates. These values were also 75% and 41% higher when compared to *Slc2a1*$^{+/-}$ littermates (**Fig 2a-c**). Western blot analysis of fibrin and IgG in vascular-depleted brain homogenates confirmed immunostaining results (**Fig 2d-f**). More progressive fibrin and IgG leakages were found in 6 month old mice compared to 2-week-old mice (**Supplementary Fig 3**), but the trend of changes observed between different genotypes remained the same as in 2 week old mice. These data suggest that GLUT1 is required for maintenance of BBB integrity in mice and that reduction in GLUT1 expression may accelerate and augment changes in vascular permeability seen with increased Aβ, such as *APP*$^{sw/0}$ mice[38].

We next studied whether the expression of the BBB tight junction proteins underlying the barrier properties of brain endothelium is altered by GLUT1 deficiency in the mammalian brain as it is in the lower vertebrate brain lacking GLUT1[11]. Immunostaining for occludin and lectin and ZO-1 and lectin indicated early and significant reductions in both tight junction proteins by approximately 40% and 50%, respectively, in *Slc2a1*$^{+/-}$ mice when compared to age-matched *Slc2a1*$^{+/+}$ littermates (**Fig 2g-h**). We also found a moderate ~20% reduction in occludin length, but not ZO-1, in *Slc2a1*$^{+/+}$*APP*$^{Sw/0}$ mice compared to age-matched *Slc2a1*$^{+/+}$ controls (**Fig 2g-h**), which may explain the increased BBB leakage in *APP*$^{Sw/0}$ mice (**Fig 2a-f**). *Slc2a1*$^{+/-}$*APP*$^{Sw/0}$ mice had significantly greater losses of occludin and ZO-1 when compared to *Slc2a1*$^{+/+}$*APP*$^{Sw/0}$ mice, suggesting that reductions in GLUT1 in the setting of an abundance of Aβ results in greater tight junctional reductions and permeability deficits. The reductions in tight junction protein expression in different mouse lines correlated well with increased BBB permeability, as illustrated by negative correlations between the extravascular fibrin and IgG deposits and the occludin capillary length (**Fig. 2j-k**), respectively, when compared to *Slc2a1*$^{+/+}$ littermate controls. Immunoblotting of isolated microvessels confirmed greatest reductions in occludin, ZO-1 and claudin-5 in 2 week old *Slc2a1*$^{+/-}$*APP*$^{Sw/0}$ mice compared to other age-matched genotypes (**Fig. 2l-m**).

GLUT1 deficiency leads to accelerated cerebral β-amyloidosis

The BBB is a critical site of transport exchanges regulating brain Aβ[1, 2]. To investigate whether diminished BBB GLUT1 expression influences progression of CNS β-amyloidosis, we analyzed Aβ pathology. $A\beta_{40}$ and $A\beta_{42}$ levels were increased by 28% and 95% and 73% and 48% increases in the cortex, and 51% and 80% and 89% and 53% in the hippocampus of 6- and 16-month-old *Slc2a1*$^{+/-}$*APP*$^{Sw/0}$ mice compared to their respective age-matched littermate controls (**Fig 3a-b**). At 1 month of age, however, Aβ levels in the cortex and hippocampus of *Slc2a1*$^{+/-}$*APP*$^{Sw/0}$ mice were not elevated (**Fig. 3a-b**), suggesting that early reductions in capillary density in these mice (**Fig. 1a-b**) are not related to Aβ, but could be due to either early postnatal and/or developmental synergistic effects of GLUT1 deficiency and *APP* overexpression. Aβ immunostaining confirmed 53% and 62% increases in cortical and hippocampal Aβ load in 16-month-old *Slc2a1*$^{+/-}$*APP*$^{Sw/0}$ compared to *Slc2a1*$^{+/+}$*APP*$^{Sw/0}$ mice, respectively (**Fig 3c-d**), suggesting that GLUT1 deficiency accelerates and exacerbates cerebral β-amyloidosis in *APP*$^{Sw/0}$ mice.

To investigate the mechanism(s) by which GLUT1 BBB transporter may influence Aβ homeostasis, we studied whether GLUT1 deficiency alters brain capillary levels of low-density lipoprotein receptor-related protein 1 (LRP1), a key Aβ clearance transporter at the BBB[1,2]. Immunoblotting revealed a significant 47% reduction in brain capillary LRP1 in 16-month-old *Slc2a1*$^{+/+}$*APP*$^{Sw/0}$ mice compared to age-matched *Slc2a1*$^{+/+}$ littermates, consistent with a previous report[39], and a more severe 75% reduction in 16-month-old *Slc2a1*$^{+/-}$*APP*$^{Sw/0}$ mice compared to age-matched *Slc2a1*$^{+/+}$ littermates (**Fig 3e**). Surprisingly, brain capillary LRP1 levels were also reduced by 26% in 16-month-old *Slc2a1*$^{+/-}$ mice compared to *Slc2a1*$^{+/+}$ age-matched littermates (**Fig 3e**). In agreement with these findings, *in vivo* hippocampal clearance assay for human $A\beta_{40}$ indicated increased $A\beta_{40}$ retention by 59% in *Slc2a1*$^{+/-}$*APP*$^{Sw/0}$ mice when compared to *Slc2a1*$^{+/+}$*APP*$^{Sw/0}$ mice in the absence of altered clearance of the metabolically inert molecule inulin (**Fig 3f**). In agreement with the observed LRP1 BBB reductions and increased $A\beta_{40}$ retention, we found ~67% reduction in BBB clearance of Aβ without changes in Aβ interstitial fluid bulk flow (**Fig 3g**). Notably, APP, soluble APP-β, β-secretase, neprilysin and insulin degrading enzyme levels were not altered in 16-month-old *Slc2a1*$^{+/-}$*APP*$^{Sw/0}$ mice compared to *Slc2a1*$^{+/+}$*APP*$^{Sw/0}$ littermates indicating that enhanced APP production and/or processing or reduced Aβ enzymatic degradation do not contribute to exacerbations in β-amyloidosis in *Slc2a1*$^{+/-}$*APP*$^{Sw/0}$ mice (**Supplementary Fig 4a-g**). Together, these data are consistent with a faulty LRP1-dependent Aβ clearance at the BBB.

To confirm that diminished LRP1-dependent Aβ clearance is critical for Aβ accumulation in *Slc2a1*$^{+/-}$*APP*$^{Sw/0}$ mice, we re-expressed LRP1 minigene (*mLRP1*)[40] in the hippocampus of *Slc2a1*$^{+/-}$*APP*$^{Sw/0}$ mice using adenoviral-mediated transfer (Ad.*mLRP1*). This led to robust expression of the LRP1 minigene in the hippocampus, particularly within blood vessels of *Slc2a1*$^{+/-}$*APP*$^{Sw/0}$ mice (**Supplementary Fig 5a-c**) resulting in significant reductions in Aβ load and $A\beta_{40}$ and $A\beta_{42}$ levels by 45%, 35% and 22% compared to the contralateral control hippocampus injected with the control empty vector, respectively (**Fig 3h-j**). These data indicate that reduced microvascular LRP1 levels contribute to diminished Aβ clearance in GLUT1-deficient *APP*$^{sw/0}$ mice in addition to reductions in brain capillary surface area and resting CBF.

To confirm that GLUT1 regulates LRP1-dependent Aβ clearance at the BBB *in vivo*, we performed a rescue experiment with GLUT1, and re-expressed GLUT1 in the hippocampus of *Slc2a1*$^{+/-}$*APP*$^{Sw/0}$ mice using adenoviral-mediated Ad.*Slca1* transfer. Compared to the control hippocampus injected with the control empty vector, Ad.*Slca1* increased the expression of both GLUT1 and LRP1 in brain microvessels (**Supplementary Fig 5d-g**), which in turn reduced the Aβ load, Aβ40 and Aβ42 levels by 37%, 45% and 33%, respectively (**Fig 3k-m**). Collectively, these data implicate that re-expression of GLUT1 in *Slc2a1*$^{+/-}$*APP*$^{Sw/0}$ mice slows down development of Aβ pathology by increasing cerebrovascular LRP1 levels.

To better understand the link between GLUT1 and LRP1, we next performed a series of experiments using primary murine brain endothelial cells (BEC). Consistent with a recent report showing that GLUT1 levels in brain microvessels in different mouse strains correlate closely with LRP1 levels, i.e., the lower the GLUT1 levels, the lower the LRP1 levels[41], and

our findings of reduced LRP1 levels in brain microvessels of *Slca1*$^{+/-}$ mice (**Fig 3e**), we found that GLUT1 inhibition with si.*Slca1* leads to transcriptional LRP1 suppression in *Slc2a1*$^{+/+}$ BEC, whereas Ad.*Slca1* adenoviral-mediated re-expression of GLUT1 in *Slca1*$^{+/-}$ BEC increases LRP1 levels (**Supplementary Fig 6a-c**). Silencing LRP1 failed to decrease GLUT1 levels (**Supplementary Fig 6d**) suggesting that changes in GLUT1 expression influence LRP1 expression.

In search of a possible molecular mechanism, we studied whether the sterol regulatory element binding protein 2 (SREBP2) – the only known transcriptional suppressor of LRP1[42,43] previously shown to inhibit LRP1 in brain vascular cells in AD and AD models[42] – is involved in mediating GLUT1 effects. si.*Slca1*-mediated GLUT1 inhibition increased SREBP2 levels and suppressed LRP1 levels in *Slc2a1*$^{+/+}$ BEC, whereas inhibition of GLUT1 in the presence of silenced SREBP2 (si.*Srebp2*) failed to suppress LRP1 (**Supplementary Fig 6e-h**). SREBP2 levels were increased in *Slca1*$^{+/-}$ BEC when compared to *Slc2a1*$^{+/+}$ BEC, which correlated with LRP1 reduction (**Supplementary Fig. 6i-k**). Together, these findings indicate that SREBP2 is critical for LRP1 suppression in BEC.

Neuronal dysfunction and cognitive impairment in *Slc2a1*$^{+/-}$*APP*$^{Sw/0}$ mice

We utilized *in vivo* voltage sensitive dye (VSD) imaging to determine evoked membrane potential responses with millisecond temporal resolution immediately following hindlimb mechanical stimulation[44]. In *Slc2a1*$^{+/+}$ mice, hindlimb stimulation evoked a robust, transient depolarization (<100 ms) originating in the contralateral hindlimb somatosensory cortex which subsequently propagated to adjacent motor and forelimb somatosensory cortices prior to returning to baseline values (**Fig 4a**). At 2 weeks of age, evoked cortical depolarization displayed no abnormalities in peak amplitude of response, as measured by peak change in fluorescence normalized to baseline fluorescence (peak $\Delta F/F_o$) and response latency in *Slc2a1*$^{+/+}$, *Slc2a1*$^{+/-}$, *Slc2a1*$^{+/+}$*APP*$^{Sw/0}$ or *Slc2a1*$^{+/-}$*APP*$^{Sw/0}$ mice (**Fig 4b, e, f**). Conversely, reductions in evoked hindlimb cortical response amplitude and prolongation of response latency were noted in *Slc2a1*$^{+/-}$*APP*$^{Sw/0}$, but not in *Slc2a1*$^{+/-}$ and *Slc2a1*$^{+/+}$*APP*$^{Sw/0}$ mice, beginning at 1 month of age, respectively (**Fig 4a,c-f**). By 6-months, cortical responses in *Slc2a1*$^{+/-}$*APP*$^{Sw/0}$ mice were substantially reduced with severely prolonged response latency (**Fig 4a,d-f**). We also found more moderate reductions in cortical activity in *Slc2a1*$^{+/-}$ and *Slc2a1*$^{+/+}$*APP*$^{Sw/0}$ mice beginning at 6 month of age (**Fig 4a, d-f**). These data demonstrate that vascular changes readily detectable at 2 weeks of age in *Slc2a1*$^{+/-}$*APP*$^{Sw/0}$ mice (Fig 1a,b; Fig 2) precede neuronal dysfunction. Similar, BBB breakdown observed early in *Slc2a1*$^{+/-}$ and *Slc2a1*$^{+/+}$*APP*$^{Sw/0}$ mice also precedes diminished evoked membrane potential responses in these mice although they develop slower than in *Slc2a1*$^{+/-}$*APP*$^{Sw/0}$ mice.

Next, we sought to evaluate function of neuronal circuitries underlying hippocampal learning and spatial memory through the assessment of novel object location (**Fig 5a**) and novel object recognition memory (**Fig 5b**). At 1-month of age, no impairment in novel object location or recognition memory was detected in 1-month-old *Slc2a1*$^{+/-}$*APP*$^{Sw/0}$ mice (**Fig 5a-b**). At 6 months of age, however, *Slc2a1*$^{+/-}$, *Slc2a1*$^{+/+}$*APP*$^{Sw/0}$ and

Slc2a1$^{+/-}$*APP*$^{Sw/0}$ mice all showed significant impairment in novel object location and recognition memory (**Fig 5a-b**). As observed with VSD imaging, novel object location and recognition memory was most severely affected in *Slc2a1*$^{+/-}$*APP*$^{Sw/0}$ mice (**Fig 5a-b**). Assessment of nest construction confirmed the onset of behavioral impairment in 6-month-old *Slc2a1*$^{+/-}$, *Slc2a1*$^{+/+}$*APP*$^{Sw/0}$ and the more severely affected *Slc2a1*$^{+/-}$*APP*$^{Sw/0}$ mice, but not at 1-month of age (**Fig 5c**). Behavioral deficits were not the result of reduced locomotor activity (**Fig 5d**). Golgi-Cox histological analysis revealed graded dendritic spine reductions in the dentate gyrus in 6-month-old *Slc2a1*$^{+/-}$, *Slc2a1*$^{+/+}$*APP*$^{Sw/0}$ and *Slc2a1*$^{+/-}$*APP*$^{Sw/0}$ mice (**Fig 5e-f**) which closely mimicked genotype-dependent impairments in hippocampal function.

GLUT1 deficiency results in neurodegenerative changes in *APP*$^{Sw/0}$ mice

Quantification of SMI-311 positive non-phosphorylated neurofilaments in the hindlimb somatosensory cortex and CA1 hippocampal subfield[44] revealed no significant differences in 1-month-old *Slc2a1*$^{+/-}$, *Slc2a1*$^{+/+}$*APP*$^{Sw/0}$ and *Slc2a1*$^{+/-}$*APP*$^{Sw/0}$ mice compared to age-matched control *Slc2a1*$^{+/+}$ littermates confirming that vascular dysfunction precedes detectable neuronal structural changes (**Fig 6a-b**). At later time points at 6 months of age, significant 18% and 22% reductions in hippocampal and cortical SMI-311 positive neurofilaments were noted in *Slc2a1*$^{+/-}$*APP*$^{Sw/0}$ mice, respectively, compared to other genotypes (**Fig 6a-b**). Significant 15% and 13% reductions in neurofilament density were detected in the cortex and hippocampus in 16-month-old *Slc2a1*$^{+/-}$ mice, but not in *Slc2a1*$^{+/+}$*APP*$^{Sw/0}$ or age-matched littermate controls, that compares to more pronounced 23% and 28% respective reductions in age-matched *Slc2a1*$^{+/-}$*APP*$^{Sw/0}$ mice (**Fig 6a-b**).

To evaluate neuronal loss, we next quantified neuron-specific nuclear protein A60 (NeuN) positive cells in the cortex and hippocampus of different mice. This quantification revealed significant 15% and 16% and 25% and 31% reductions in hippocampal and cortical NeuN-positive cells in 6- and 16-month-old *Slc2a1*$^{+/-}$*APP*$^{Sw/0}$ mice, respectively (**Fig 6c-d**). No changes were observed in other genotypes within 6 months of age. Significant 13% and 14% reductions in NeuN-positive cells were detected, however, in the CA1 hippocampal subfield and somatosensory cortex, respectively, at a later stage in 16-month-old *Slc2a1*$^{+/-}$ mice (**Fig 6c-d**). Consistent with a previous report[45], we did not find a significant neuronal loss in *Slc2a1*$^{+/+}$*APP*$^{Sw/0}$ mice at all-time points analyzed (**Fig 6c-d**).

We also analyzed whether there was gross alterations in brain architecture through measurement of mean cortical diameter, an index of brain size. This analysis demonstrated significant 4% and more severe 7% reductions in 6-month-old *Slc2a1*$^{+/-}$ and *Slc2a1*$^{+/-}$*APP*$^{Sw/0}$ mice, respectively, but no significant alterations in brain size in *Slc2a1*$^{+/+}$*APP*$^{Sw/0}$ mice (**Fig 6e-f**).

GLUT1 deficiency in endothelium initiates vascular BBB changes

Brain microvessels from *Slc2a1*$^{+/+}$ mice express 55 kDa GLUT1 endothelial isoform[3], whereas capillary-depleted brain homogenates containing astrocytes and neurons, but not microvessels (as shown by multiple cell-specific markers on immunoblots), express 45 kDa GLUT1 astrocytic isoform[3] at very low levels (**Supplementary Fig. 7a-c**). When compared

to the 55 kDa isoform, the levels of the 45 kDa GLUT1 isoform were approximately 26-fold lower. In *Slca1*$^{+/-}$ mice compared to *Slc2a1*$^{+/+}$ controls, we found >50% and 40% losses of the 55 and 45 kDa GLUT1, respectively (**Supplementary Fig 7d-e**). Moreover, in the capillary-depleted brains of *Slca1*$^{+/-}$ mice compared to *Slc2a1*$^{+/+}$ mice, we detected a ~2-fold increase in GLUT2 levels, a glucose transporter that is expressed in astrocytes[3,46], and a 2.6-fold increase in GLUT3 levels, a glucose transporter that is expressed in neurons[46,47], suggesting metabolic adaptations in different cell types in the presence of GLUT1 deficiency (**Supplementary Fig 7f-g**).

Using primary murine BEC and astrocytes from *Slc2a1*$^{+/+}$ mice, we confirmed that the 55 kDa GLUT1 in BEC is expressed at significantly higher levels by ~20-fold compared to the 45 kDa GLUT1 in astrocytes (**Supplementary Fig. 7h**) and that GLUT1 haploinsuficiency leads to ~60% loss of GLUT1 from BEC and >40% loss of GLUT1 from astrocytes, and a 3.5-fold increase in GLUT2 levels in astrocytes (**Supplementary Fig 7i-j**). Thus, global GLUT1 deficiency leads to a critical loss of glucose transporters from endothelium that likely has a major effect on the vascular phenotype in *Slca1*$^{+/-}$ mice. In contrast, astrocytes express substantially lower levels of GLUT1 at baseline, and during GLUT1 global deficiency maintain less significant loss of glucose transporters, as indicated by relatively smaller loss of GLUT1 and a compensatory increase in GLUT2.

Then, we took advantage of conditional *Slc2a1* $^{lox/lox}$ mice[31] and generated *Slc2a1* $^{lox/+}$; *Tie2-Cre*$^{+/0}$ and *Slc2a1* $^{lox/+}$; *GFAP-Cre*$^{+/0}$ mice with partial GLUT1 deletions from endothelium and astrocytes, respectively, to determine their respective effects on the BBB integrity that we show is compromised early in *Slca1*$^{+/-}$ mice at 2 weeks of age (**Fig. 2**). As expected, we found diminished levels of GLUT1 in endothelium in *Slc2a1* $^{lox/+}$; *Tie2-Cre*$^{+/0}$ mice by double immunostaining for GLUT1 and lectin-positive endothelial profiles (>40%) and immunoblotting for 55 kDa endothelial isoform in isolated brain microvessels (~45%), but no change in the astrocyte-associated 45 kDa isoform in capillary-depleted brains (**Supplementary Fig. 8a-d**). In contrast, *Slc2a1* $^{lox/+}$; *GFAP-Cre*$^{+/0}$ mice did not have loss of GLUT1 from endothelium, confirming that GLUT1 deletion from astrocytes does not affect function of endothelial GLUT1. In *Slc2a1* $^{lox/+}$; *GFAP-Cre*$^{+/0}$ mice, GLUT1 was undetectable in brain parenchyma by immunostaining as reported[3], but there was >50% loss of 45 kDa isoform in the astrocyte-containing capillary-depleted brains (**Supplementary Fig 8d**).

We next found the BBB breakdown in endothelial GLUT1-deficient *Slc2a1* $^{lox/+}$; *Tie2-Cre*$^{+/0}$ mice, but not in astrocyte GLUT1-deficient *Slc2a1* $^{lox/+}$; *GFAP-Cre*$^{+/0}$ mice, as shown by 10- and 15-fold greater extravascular accumulation of fibrin and IgG in brain parenchyma (**Fig 7a-c**), and 45% and 47% reductions in the lengh of the BBB tight junction proteins occludin and ZO-1, respectively (**Fig 7d-f**), in *Slc2a1* $^{lox/+}$; *Tie2-Cre*$^{+/0}$ mice compared to *Slc2a1* $^{lox/+}$ littermate controls. In contrast, GLUT1-deficiency in astrocytes in *Slc2a1* $^{lox/+}$; *GFAP-Cre*$^{+/0}$ mice did not result in BBB breakdown. A decrease in the occludin length in *Slc2a1* $^{lox/+}$; *Tie2-Cre*$^{+/0}$ mice correlated with increased BBB breakdown to fibrin and IgG (**Fig 7g-h**), when compared to *Slc2a1* $^{lox/+}$; *GFAP-Cre*$^{+/0}$ mice and *Slc2a1* $^{lox/+}$ littermate controls. Collectively, these data indicate that GLUT1 deficiency in endothelium, but not astrocytes, initiates the vascular phenotype with BBB breakdown.

GLUT1 deficiency in red blood cells does not contribute to central effects

GLUT1 is present in red blood cells (RBC)[46]. Our data show that *Slc2a1* haplosufficiency does not affect RBC indices and hemoglobin oxygen saturation and dissociation in $Slca1^{+/-}$, $Slc2a1^{+/+}APP^{Sw/0}$ and $Slc2a1^{+/-}APP^{Sw/0}$ mice. We found moderate 23% reduction in GLUT1 membrane protein levels in RBC's from $Slc2a1^{+/-}$ mice likely due to compensatory upregulation (**Supplementary Fig 9a**). RBCs in $Slc2a1^{+/+}$, $Slca1^{+/-}$, $Slc2a1^{+/+}APP^{Sw/0}$ and $Slc2a1^{+/-}APP^{Sw/0}$ mice had normal shape (**Supplementary Fig 9b**) and normal mechanical properties under shear stress conditions (1.5-50 Pascal) (**Supplementary Fig 9c**). $Slc2a1^{+/+}$, $Slca1^{+/-}$, $Slc2a1^{+/+}APP^{Sw/0}$ and $Slc2a1^{+/-}APP^{Sw/0}$ mice all had normal hematological parameters such as the amount of hemoglobin, average RBC size, the amount of hemoglobin per RBC, the amount of hemoglobin relative to the size of the cell, and red cell distribution width, as well as normal saturation level of oxygen in hemoglobin and P50 value of oxygen dissociation (**Supplementary Fig. 9d-l**). These data suggest that peripheral changes in RBCs do not make significant contributions to the observed effects within the brain.

Discussion

We show that GLUT1 in addition to its well known role in transporting glucose into the brain[1,2] is necessary for the maintenance of proper brain capillary networks, blood flow and BBB integrity, as well as neuronal function and structure (Supplementary **Fig 10**). Capillary degeneration and BBB breakdown occur early in AD mice with GLUT1 deficiency ($Slc2a1^{+/-}APP^{Sw/0}$) at 2 weeks of age, and are associated with reduced brain perfusion and diminished glucose uptake into the brain, whereas neuronal dysfunction, behavioral deficits, elevated Aβ levels and behavioral and neurodegenerative changes develop later within 6 months of age.

GLUT1 deficiency in endothelium, but not astrocytes, initiates the vascular phenotype with BBB breakdown. Besides reductions in the tight junction proteins, early metabolic changes in the endothelium due to reduced glucose uptake might contribute to endothelial cell injury and BBB breakdown. Loss of GLUT1 from brain endothelium generates multiple parallel pathogenic mechanisms in the cerebral microcirculation, which can contribute to the observed neuronal dysfunction and neurodegeneration. Each of these vascular insults alone, i.e., the BBB breakdown, diminished BBB glucose transport, CBF reductions, capillary degeneration, neurovascular uncoupling and impaired Aβ BBB clearance, may be independently neuronal toxic, but their synergism likely amplifies the overall pathogenic effects of GLUT1 deficiency.

Metabolic stress due to chronically reduced glucose levels in brain, if not compensated, may lead to neuronal and glial hypometabolism and oxidative stress, which can contribute to neurotoxicity[48]. Additionally, shifts in metabolism can take place in different cell types within the neurovascular unit, and at different stages during limited glucose availability. The metabolic pathways through which BBB GLUT1 reductions influence brain metabolism, including endothelial glucose metabolism, the astrocyte lactate shuttle and/or oxidative metabolism, and neuronal supply, are presently unknown and likely represent an important focus for future studies.

When combined with *APP* overexpression, GLUT1 reduction results in early neurodegeneration marked by the retraction of neurites, neuronal loss and substantial behavioral deficits at 6 months of age that are not seen in $APP^{Sw/0}$ mice as shown in the present and earlier reports[45,49]. GLUT1 deficiency leads to reductions in Aβ-clearance and accelerates Aβ pathology via reduced expression of LRP1 in the microvasculature. Importantly, these changes are reversible as demonstrated by the GLUT1 and LRP1 rescue experiments in the hippocampus. Therefore, neuronal loss in $Slc2a1^{+/-}APP^{Sw/0}$ mice, likely reflects synergistic effects of GLUT1-mediated vascular injury, diminished neuronal glucose delivery, and greater accumulation of Aβ neurotoxic species at the neuronal interface.

Our data using GLUT1 deficient mice with an early embryonic loss of GLUT1 suggest that GLUT1 may fulfill an important regulatory role in the microcirculation and Aβ clearance in the adult and aging brain. Future studies using murine models with inducible GLUT1 loss from endothelium might address whether there is a difference in the CNS response to an early embryonic GLUT1 loss compared to a later GLUT1 loss from brain. Interestingly, adult patients with GLUT1-deficiency syndrome[50] do not show clinical evidence for AD. Whether GLUT1-deficiency can accelerate cognitive decline during aging in humans remains, however, to be seen. The present data suggest that GLUT1 deficiency can contribute to a disease process acting in tandem with Aβ to initiate and/or amplify vascular damage and Aβ accumulation.

The two-hit vascular hypothesis of Alzheimer's disease states that early vascular injury leads to BBB compromise and perfusion stress which can initiate Aβ-independent and Aβ-dependent mechanisms of neurotoxicity[2]. Here, we show that GLUT1 transporter at the BBB influences both Aβ-independent and Aβ-dependent neuronal injury. The molecular mechanisms governing GLUT1 reductions in AD and whether these may be pharmacologically targeted to restore GLUT1 expression remain unknown. Nevertheless, our data suggest that GLUT1 is an important therapeutic target for AD-related neurovascular dysfunction and neurodegeneration.

Supplementary Material

Refer to Web version on PubMed Central for supplementary material.

Acknowledgments

This research was supported by the National Institute of Health grants AG039452, AG023084 and NS034467 to B.V.Z. and U01 HL087947 and R01DK092065 to E.D.A. We thank Dr. Elyse Schauwecker for most helpful discussion.

References

1. Zlokovic BV. The blood-brain barrier in health and chronic neurodegenerative disorders. Neuron. 2008; 57:178–201. [PubMed: 18215617]
2. Zlokovic BV. Neurovascular pathways to neurodegeneration in Alzheimer's disease and other disorders. Nat. Rev. Neurosci. 2011; 12:723–738. [PubMed: 22048062]
3. Simpson IA, Carruthers A, Vannucci SJ. Supply and demand in cerebral energy metabolism: the role of nutrient transporters. J. Cereb. Blood Flow Metab. Off. J. Int. Soc. Cereb. Blood Flow Metab. 2007; 27:1766–1791.

4. Deng D, et al. Crystal structure of the human glucose transporter GLUT1. Nature. 2014; 510:121–125. [PubMed: 24847886]
5. Allen A, Messier C. Plastic changes in the astrocyte GLUT1 glucose transporter and beta-tubulin microtubule protein following voluntary exercise in mice. Behav. Brain Res. 2013; 240:95–102. [PubMed: 23201358]
6. Choeiri C, Staines W, Miki T, Seino S, Messier C. Glucose transporter plasticity during memory processing. Neuroscience. 2005; 130:591–600. [PubMed: 15590143]
7. Zeller K, Rahner-Welsch S, Kuschinsky W. Distribution of Glut1 glucose transporters in different brain structures compared to glucose utilization and capillary density of adult rat brains. J. Cereb. Blood Flow Metab. Off. J. Int. Soc. Cereb. Blood Flow Metab. 1997; 17:204–209.
8. Pearson TS, Akman C, Hinton VJ, Engelstad K, De Vivo DC. Phenotypic spectrum of glucose transporter type 1 deficiency syndrome (Glut1 DS). Curr. Neurol. Neurosci. Rep. 2013; 13:342. [PubMed: 23443458]
9. Wang D, et al. A mouse model for Glut-1 haploinsufficiency. Hum. Mol. Genet. 2006; 15:1169–1179. [PubMed: 16497725]
10. Ullner PM, et al. Murine Glut-1 transporter haploinsufficiency: postnatal deceleration of brain weight and reactive astrocytosis. Neurobiol. Dis. 2009; 36:60–69. [PubMed: 19591936]
11. Zheng P-P, et al. Glut1/SLC2A1 is crucial for the development of the blood-brain barrier in vivo. Ann. Neurol. 2010; 68:835–844. [PubMed: 21194153]
12. Nguyen LN, et al. Mfsd2a is a transporter for the essential omega-3 fatty acid docosahexaenoic acid. Nature. 2014; 509:503–506. [PubMed: 24828044]
13. Ben-Zvi A, et al. Mfsd2a is critical for the formation and function of the blood-brain barrier. Nature. 2014; 509:507–511. [PubMed: 24828040]
14. Zhao Z, Zlokovic BV. Blood-brain barrier: a dual life of MFSD2A? Neuron. 2014; 82:728–730. [PubMed: 24853933]
15. Landau SM, et al. Amyloid deposition, hypometabolism, and longitudinal cognitive decline. Ann. Neurol. 2012; 72:578–586. [PubMed: 23109153]
16. Winkler EA, Sagare AP, Zlokovic BV. The pericyte: a forgotten cell type with important implications for Alzheimer's disease? Brain Pathol. Zurich Switz. 2014; 24:371–386.
17. Ossenkoppele R, et al. Differential effect of APOE genotype on amyloid load and glucose metabolism in AD dementia. Neurology. 2013; 80:359–365. [PubMed: 23255822]
18. Protas HD, et al. Posterior cingulate glucose metabolism, hippocampal glucose metabolism, and hippocampal volume in cognitively normal, late-middle-aged persons at 3 levels of genetic risk for Alzheimer disease. JAMA Neurol. 2013; 70:320–325. [PubMed: 23599929]
19. Mosconi L, et al. Amyloid and metabolic positron emission tomography imaging of cognitively normal adults with Alzheimer's parents. Neurobiol. Aging. 2013; 34:22–34. [PubMed: 22503001]
20. Landau SM, et al. Comparing predictors of conversion and decline in mild cognitive impairment. Neurology. 2010; 75:230–238. [PubMed: 20592257]
21. Mosconi L, et al. FDG-PET changes in brain glucose metabolism from normal cognition to pathologically verified Alzheimer's disease. Eur. J. Nucl. Med. Mol. Imaging. 2009; 36:811–822. [PubMed: 19142633]
22. Mosconi L, et al. Hypometabolism exceeds atrophy in presymptomatic early-onset familial Alzheimer's disease. J. Nucl. Med. Off. Publ. Soc. Nucl. Med. 2006; 47:1778–1786.
23. Niwa K, Kazama K, Younkin SG, Carlson GA, Iadecola C. Alterations in cerebral blood flow and glucose utilization in mice overexpressing the amyloid precursor protein. Neurobiol. Dis. 2002; 9:61–68. [PubMed: 11848685]
24. Jagust WJ, et al. Diminished glucose transport in Alzheimer's disease: dynamic PET studies. J. Cereb. Blood Flow Metab. Off. J. Int. Soc. Cereb. Blood Flow Metab. 1991; 11:323–330.
25. Piert M, Koeppe RA, Giordani B, Berent S, Kuhl DE. Diminished glucose transport and phosphorylation in Alzheimer's disease determined by dynamic FDG-PET. J. Nucl. Med. Off. Publ. Soc. Nucl. Med. 1996; 37:201–208.

26. Simpson IA, Chundu KR, Davies-Hill T, Honer WG, Davies P. Decreased concentrations of GLUT1 and GLUT3 glucose transporters in the brains of patients with Alzheimer's disease. Ann. Neurol. 1994; 35:546–551. [PubMed: 8179300]
27. Mooradian AD, Chung HC, Shah GN. GLUT-1 expression in the cerebra of patients with Alzheimer's disease. Neurobiol. Aging. 1997; 18:469–474. [PubMed: 9390772]
28. Kalaria RN, Harik SI. Reduced glucose transporter at the blood-brain barrier and in cerebral cortex in Alzheimer disease. J. Neurochem. 1989; 53:1083–1088. [PubMed: 2769254]
29. Horwood N, Davies DC. Immunolabelling of hippocampal microvessel glucose transporter protein is reduced in Alzheimer's disease. Virchows Arch. Int. J. Pathol. 1994; 425:69–72.
30. Hsiao K, et al. Correlative memory deficits, Abeta elevation, and amyloid plaques in transgenic mice. Science. 1996; 274:99–102. [PubMed: 8810256]
31. Young CD, et al. Modulation of glucose transporter 1 (GLUT1) expression levels alters mouse mammary tumor cell growth in vitro and in vivo. PloS One. 2011; 6:e23205. [PubMed: 21826239]
32. Deane R, et al. RAGE mediates amyloid-beta peptide transport across the blood-brain barrier and accumulation in brain. Nat. Med. 2003; 9:907–913. [PubMed: 12808450]
33. Paris D, et al. Impaired angiogenesis in a transgenic mouse model of cerebral amyloidosis. Neurosci. Lett. 2004; 366:80–85. [PubMed: 15265595]
34. Paris D, et al. Inhibition of angiogenesis by Abeta peptides. Angiogenesis. 2004; 7:75–85. [PubMed: 15302999]
35. Abdul Muneer PM, Alikunju S, Szlachetka AM, Murrin LC, Haorah J. Impairment of brain endothelial glucose transporter by methamphetamine causes blood-brain barrier dysfunction. Mol. Neurodegener. 2011; 6:23. [PubMed: 21426580]
36. Iadecola C, et al. SOD1 rescues cerebral endothelial dysfunction in mice overexpressing amyloid precursor protein. Nat. Neurosci. 1999; 2:157–161. [PubMed: 10195200]
37. Niwa K, et al. Abeta 1-40-related reduction in functional hyperemia in mouse neocortex during somatosensory activation. Proc. Natl. Acad. Sci. U. S. A. 2000; 97:9735–9740. [PubMed: 10944232]
38. Paul J, Strickland S, Melchor JP. Fibrin deposition accelerates neurovascular damage and neuroinflammation in mouse models of Alzheimer's disease. J. Exp. Med. 2007; 204:1999–2008. [PubMed: 17664291]
39. Deane R, et al. LRP/amyloid beta-peptide interaction mediates differential brain efflux of Abeta isoforms. Neuron. 2004; 43:333–344. [PubMed: 15294142]
40. Obermoeller-McCormick LM, et al. Dissection of receptor folding and ligand-binding property with functional minireceptors of LDL receptor-related protein. J. Cell Sci. 2001; 114:899–908. [PubMed: 11181173]
41. Uchida Y, et al. A study protocol for quantitative targeted absolute proteomics (QTAP) by LC-MS/MS: application for inter-strain differences in protein expression levels of transporters, receptors, claudin-5, and marker proteins at the blood-brain barrier in ddY, FVB, and C57BL/6J mice. Fluids Barriers CNS. 2013; 10:21. [PubMed: 23758935]
42. Bell RD, et al. SRF and myocardin regulate LRP-mediated amyloid-beta clearance in brain vascular cells. Nat. Cell Biol. 2009; 11:143–153. [PubMed: 19098903]
43. Llorente-Cortés V, Costales P, Bernués J, Camino-Lopez S, Badimon L. Sterol regulatory element-binding protein-2 negatively regulates low density lipoprotein receptor-related protein transcription. J. Mol. Biol. 2006; 359:950–960. [PubMed: 16697011]
44. Bell RD, et al. Apolipoprotein E controls cerebrovascular integrity via cyclophilin A. Nature. 2012; 485:512–516. [PubMed: 22622580]
45. Irizarry MC, McNamara M, Fedorchak K, Hsiao K, Hyman BT. APPSw transgenic mice develop age-related A beta deposits and neuropil abnormalities, but no neuronal loss in CA1. J. Neuropathol. Exp. Neurol. 1997; 56:965–973. [PubMed: 9291938]
46. Benarroch EE. Brain glucose transporters: implications for neurologic disease. Neurology. 2014; 82:1374–1379. [PubMed: 24647029]
47. Vannucci SJ. Developmental expression of GLUT1 and GLUT3 glucose transporters in rat brain. J. Neurochem. 1994; 62:240–246. [PubMed: 8263524]

48. Bolaños JP, Delgado-Esteban M, Herrero-Mendez A, Fernandez-Fernandez S, Almeida A. Regulation of glycolysis and pentose-phosphate pathway by nitric oxide: impact on neuronal survival. Biochim. Biophys. Acta. 2008; 1777:789–793. [PubMed: 18455501]

49. Sagare AP, et al. Pericyte loss influences Alzheimer-like neurodegeneration in mice. Nat. Commun. 2013; 4:2932. [PubMed: 24336108]

50. Seidner G, et al. GLUT-1 deficiency syndrome caused by haploinsufficiency of the blood-brain barrier hexose carrier. Nat. Genet. 1998; 18:188–191. [PubMed: 9462754]

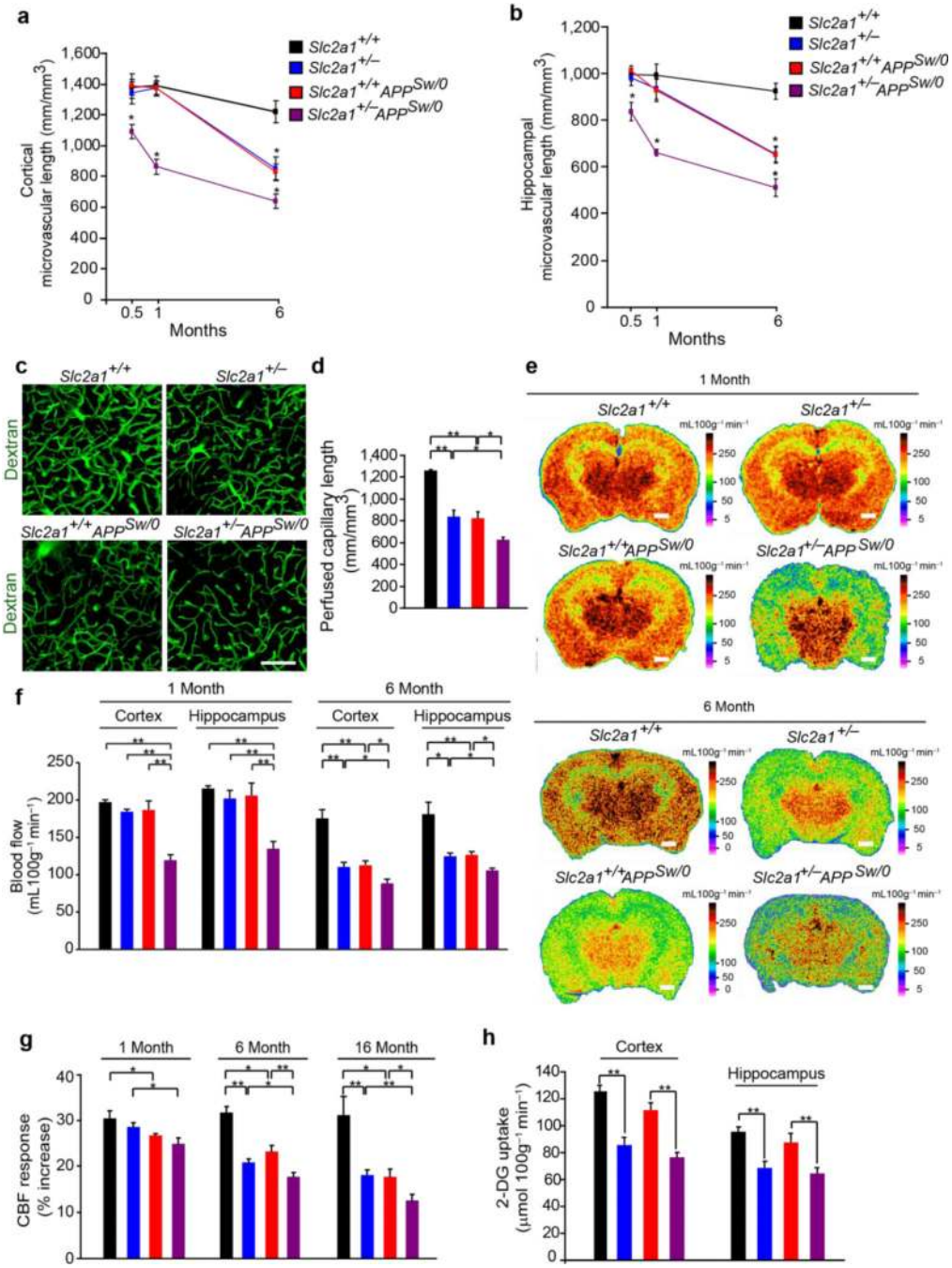

Figure 1. Microvascular and cerebral blood flow reductions and diminished glucose uptake in GLUT1-deficient *APP*$^{Sw/0}$ mice

(**a-b**) Quantification of lectin-positive microvascular profiles in cortex (**b**) and hippocampus (**b**) in 2-week, 1- and 6-month old *Slc2a1*$^{+/+}$, *Slc2a1*$^{+/-}$, *Slc2a1*$^{+/+}$*APP*$^{Sw/0}$ and *Slc2a1*$^{+/-}$*APP*$^{Sw/0}$ mice. Mean ± SEM, n=3-6 mice per group; *p<0.05. (**c-d**) Representative *in vivo* multiphoton fluorescent angiograms obtained following intravascular injection of fluorescein-conjugated dextran (MW: 70 kDa) **(c)** and quantification of perfused microvascular length (**d**) in 6-month-old *Slc2a1*$^{+/+}$, *Slc2a1*$^{+/-}$, *Slc2a1*$^{+/+}$*APP*$^{Sw/0}$ and

Slc2a1$^{+/-}$*APP*$^{Sw/0}$ mice. Scale bar, 50 μm. Mean ± SEM, n=3-4 mice per group; *p<0.05 or **p<0.01 (**e-f**) Representative C^{14}-iodoantipyrine (C^{14}-IAP) autoradiography (**e**) and quantification of C^{14}-IAP autoradiograms measuring regional blood flow in the somatosensory cortex and CA1 hippocampal subfield (**f**) in 1- and 6-month-old *Slc2a1*$^{+/+}$, *Slc2a1*$^{+/-}$, *Slc2a1*$^{+/+}$*APP*$^{Sw/0}$ and *Slc2a1*$^{+/-}$*APP*$^{Sw/0}$ mice. Scale bar, 1 mm. Mean ± SEM, n=3-5 mice per group; *p<0.05 or **p<0.01. (**g**) Cerebral blood flow (CBF) responses to brain activation in the somatosensory cortex of 1-month, 6-month and 16-month old *Slc2a1*$^{+/+}$, *Slc2a1*$^{+/-}$, *Slc2a1*$^{+/+}$*APP*$^{Sw/0}$ and *Slc2a1*$^{+/-}$*APP*$^{Sw/0}$ mice. (**h**) Quantification of C^{14}-2-deoxyglucose (2-DG) autoradiograms measuring regional glucose uptake in the somatosensory cortex and CA1 hippocampal subfield in 2-3 week-old *Slc2a1*$^{+/+}$, *Slc2a1*$^{+/-}$, *Slc2a1*$^{+/+}$*APP*$^{Sw/0}$ and *Slc2a1*$^{+/-}$*APP*$^{Sw/0}$ mice. Mean ± SEM, n=5-7 mice per group in a, b, d, f and g; and n=3 mice per group in h; *p<0.05 or **p<0.01.

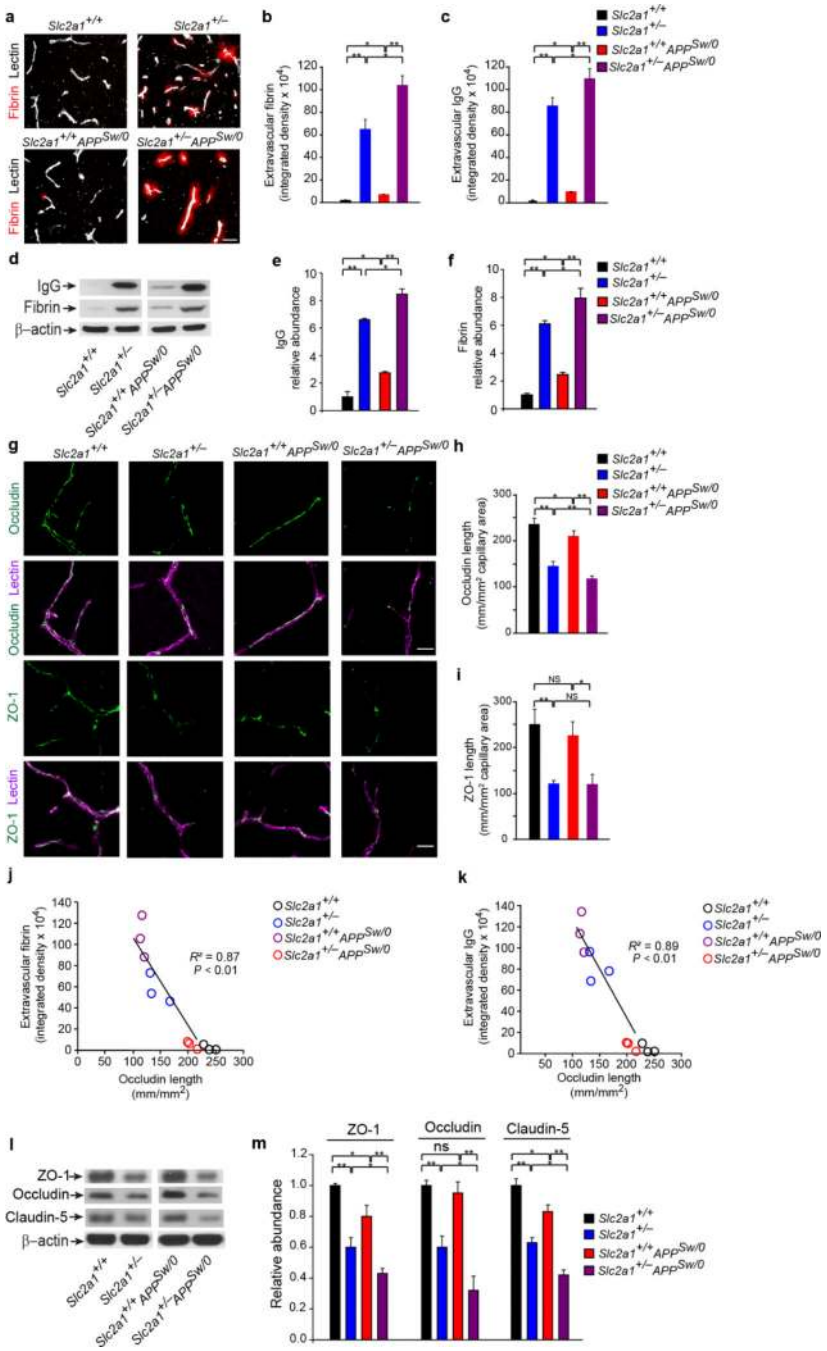

Figure 2. GLUT1 deficiency leads to early BBB breakdown in *Slc2a1*$^{+/-}$ and *Slc2a1*$^{+/-}$*APP*$^{Sw/0}$ mice

(**a**) Representative confocal microscopy analysis of fibrin (red) and lectin-positive capillaries (white) in 2-week-old *Slc2a1*$^{+/+}$,*Slc2a1*$^{+/-}$, *Slc2a1*$^{+/+}$*APP*$^{Sw/0}$ and *Slc2a1*$^{+/-}$*APP*$^{Sw/0}$ mice. Scale bar, 25 μm. (**b-c**) Quantification of extravascular fibrin (**b**) and immunoglobulin G (IgG) (**c**) deposits in 2-week old *Slc2a1*$^{+/+}$, *Slc2a1*$^{+/-}$, *Slc2a1*$^{+/+}$*APP*$^{Sw/0}$ and *Slc2a1*$^{+/-}$*APP*$^{Sw/0}$ mice. Mean ± SEM, n=3-5 mice per group; *p<0.05 or **p<0.01. (**d-f**) Representative immunoblotting of fibrin and IgG levels in

capillary-depleted brain tissue (**d**) and quantification of IgG (**e**) and fibrin (**f**) relative abundance in capillary-depleted brains in 2-week-old *Slc2a1*$^{+/+}$, *Slc2a1*$^{+/-}$, *Slc2a1*$^{+/+}$*APP*$^{Sw/0}$ and *Slc2a1*$^{+/-}$*APP*$^{Sw/0}$ mice. β-actin was used as a loading control. Mean ± SEM, n=3-5 mice per group; **p<0.01. (**g-i**) The tight junction proteins occludin or zonula occludens-1 (ZO-1) (green) and lectin-positive capillary profiles (red) (**g**) and quantification of endothelial occludin (**h**) and ZO-1 (**i**) length in the microvessels in 2-week-old *Slc2a1*$^{+/+}$, *Slc2a1*$^{+/-}$, *Slc2a1*$^{+/+}$*APP*$^{Sw/0}$ and *Slc2a1*$^{+/-}$*APP*$^{Sw/0}$ mouse hippocampus. Scale bar, 25 μm. Mean ± SEM, n=3-5 mice per group; *p<0.05 or **p<0.01. (**j-k**) Negative correlation between the extracellular fibrin (**j**) or IgG deposits (**k**) and decreased occludin length in the microvessels in 2-week-old *Slc2a1*$^{+/+}$, *Slc2a1*$^{+/-}$, *Slc2a1*$^{+/+}$*APP*$^{Sw/0}$ and *Slc2a1*$^{+/-}$*APP*$^{Sw/0}$ mouse hippocampus. (**l**) Representative immunoblotting analysis of microvascular ZO-1, occludin and claudin-5 (**l**) and their respective protein abundance in microvessels (**m**) in a 2-week-old *Slc2a1*$^{+/+}$, *Slc2a1*$^{+/-}$, *Slc2a1*$^{+/+}$*APP*$^{Sw/0}$ and *Slc2a1*$^{+/-}$*APP*$^{Sw/0}$ mouse. β-actin was used as loading control. Mean ± SEM, n=3-5 mice per group; *p<0.05 or **p<0.01. Full length blots are presented in Supplementary Figure 11.

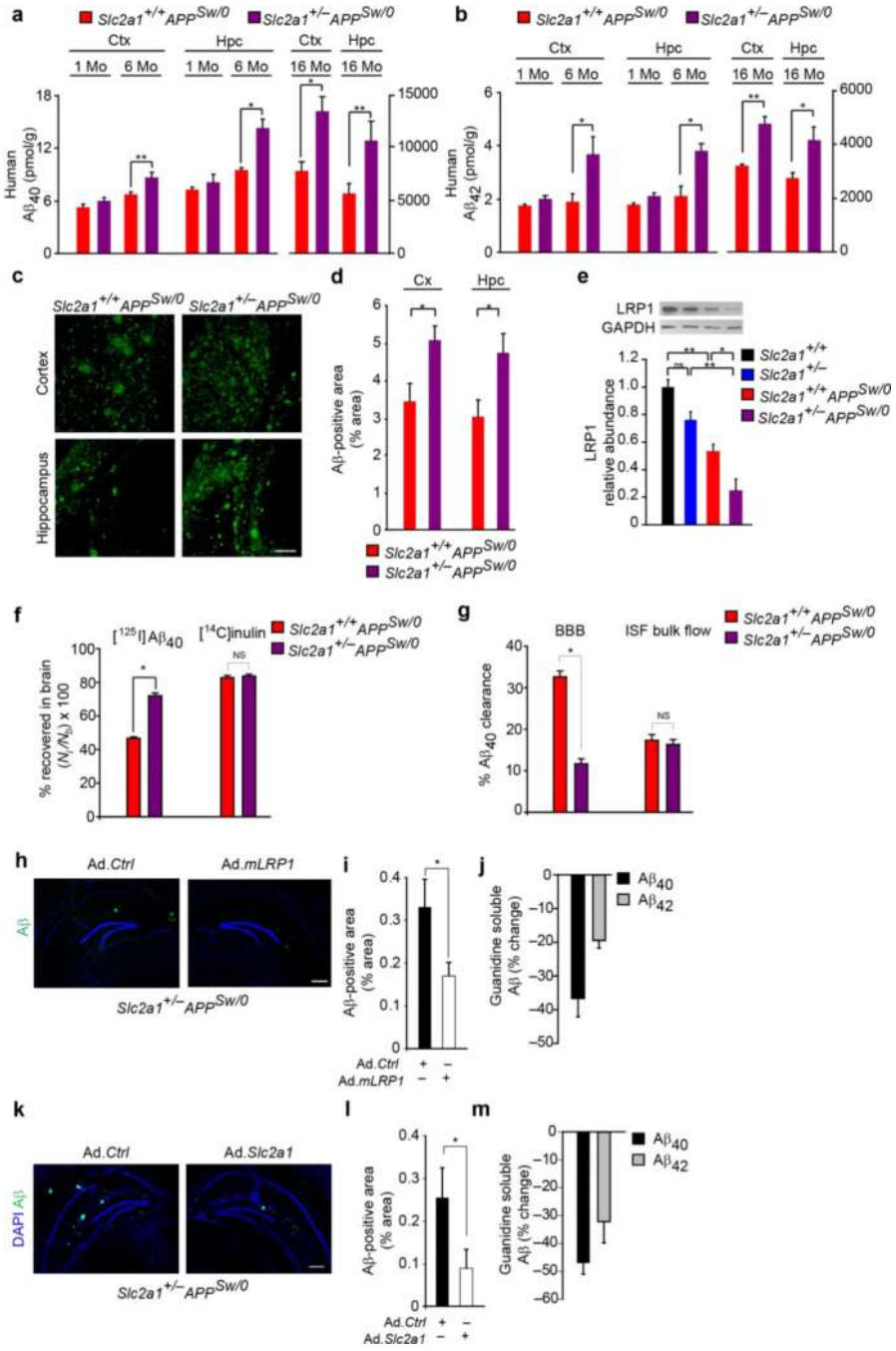

Figure 3. Aβ pathology in GLUT1-deficient *APP$^{Sw/0}$* mice and reversal by LRP1 and GLUT1 re-expression

(**a-b**) Cortical and hippocampal $A\beta_{40}$ (**a**) and $A\beta_{42}$ (**b**) levels in 1-, 6- and 16-month old *Slc2a1$^{+/+}$APP$^{Sw/0}$* and *Slc2a1$^{+/-}$APP$^{Sw/0}$* mice. Mean ± SEM, n=3-6 mice per group; *p<0.05 or **p<0.01. (**c-d**) Aβ-immunodetection (green) in the somatosensory cortex and CA1 hippocampal subfield (**c**) and Aβ load (**d**) in 16-month old *Slc2a1$^{+/+}$APP$^{Sw/0}$* and *Slc2a1$^{+/-}$APP$^{Sw/0}$* mice. Scale bar, 200 μm. Mean ± SEM, n=4-5 mice per group; *p<0.01. (**e**) Immunoblotting for the low-density lipoprotein receptor-related protein 1 (LRP1) in isolated microvessels (upper panel) and quantification (lower panel) in 16-month-old

Slc2a1$^{+/+}$, *Slc2a1*$^{+/-}$, *Slc2a1*$^{+/+}$*APP*$^{Sw/0}$ and *Slc2a1*$^{+/-}$*APP*$^{Sw/0}$ mice. Mean ± SEM, n=4 mice per group; *p<0.05 or **p<0.01. (**f**) Clearance of [^{125}I]-labeled human synthetic Aβ_{40} from CA1 hippocampal subfield in 16-month-old *Slc2a1*$^{+/+}$*APP*$^{Sw/0}$ and *Slc2a1*$^{+/-}$*APP*$^{Sw/0}$ mice. [^{14}C]inulin was used to assess brain interstitial fluid (ISF) bulk flow. Time, 30 minutes post-injection. Mean ± SEM, n=3-5 mice per group; *p<0.05. (**g**) [^{125}I]-Aβ_{40} clearance via BBB and ISF bulk flow (from the data shown in **f**). (**h-i**) Aβ-immunodetection (green) in CA1 hippocampal subfield (**h**) and quantification of Aβ-positive area (**i**) in 10-month-old *Slc2a1*$^{+/-}$*APP*$^{Sw/0}$ mouse injected with empty adenovirus (Ad.*Ctrl*) and adenovirus carrying *LRP1* minigene (Ad.*mLRP1*). Black, Ad.*Ctrl* hippocampus; White, Ad.*mLRP1* hippocampus. Scale bar, 300 μm. Mean ± SEM, n=3 mice; **p<0.01. (**j**) CA1 hippocampal guanidine soluble Aβ_{40} (black) and Aβ_{42} (grey) levels in 10-month old *Slc2a1*$^{+/-}$*APP*$^{Sw/0}$ mice injected with Ad.*Ctrl* and Ad.*mLRP1*. Graph - percent change of Ad.*mLRP1* hippocampus to Ad.*Ctrl* hippocampus. Mean ± SEM, n=3 mice per group; *p<0.05. (**k-m**) Aβ-immunodetection (green) in CA1 hippocampal subfield (**k**) and quantification of Aβ-positive area (**l**) in 8-10-month-old *Slc2a1*$^{+/-}$*APP*$^{Sw/0}$ mouse injected with empty adenovirus (Ad.*Ctrl*) and adenovirus carrying *Slc2a1* gene (Ad.*Slc2a1*). Black, Ad.*Ctrl* hippocampus; White, Ad.*Slc2a1* hippocampus. Scale bar, 300 μm. Mean ± SEM, n=3 mice; *p<0.05. (**m**) CA1 hippocampal guanidine soluble Aβ_{40} (black) and Aβ_{42} (grey) levels in 8-10-month-old *Slc2a1*$^{+/-}$*APP*$^{Sw/0}$ mice injected with Ad.*Ctrl* and Ad.*Slc2a1*. Graph - percent change of Ad.*Slc2a1* hippocampus to Ad.*Ctrl* hippocampus. Mean ± SEM, n=3 mice; *p<0.05. Full length blots are presented in Supplementary Figure 11.

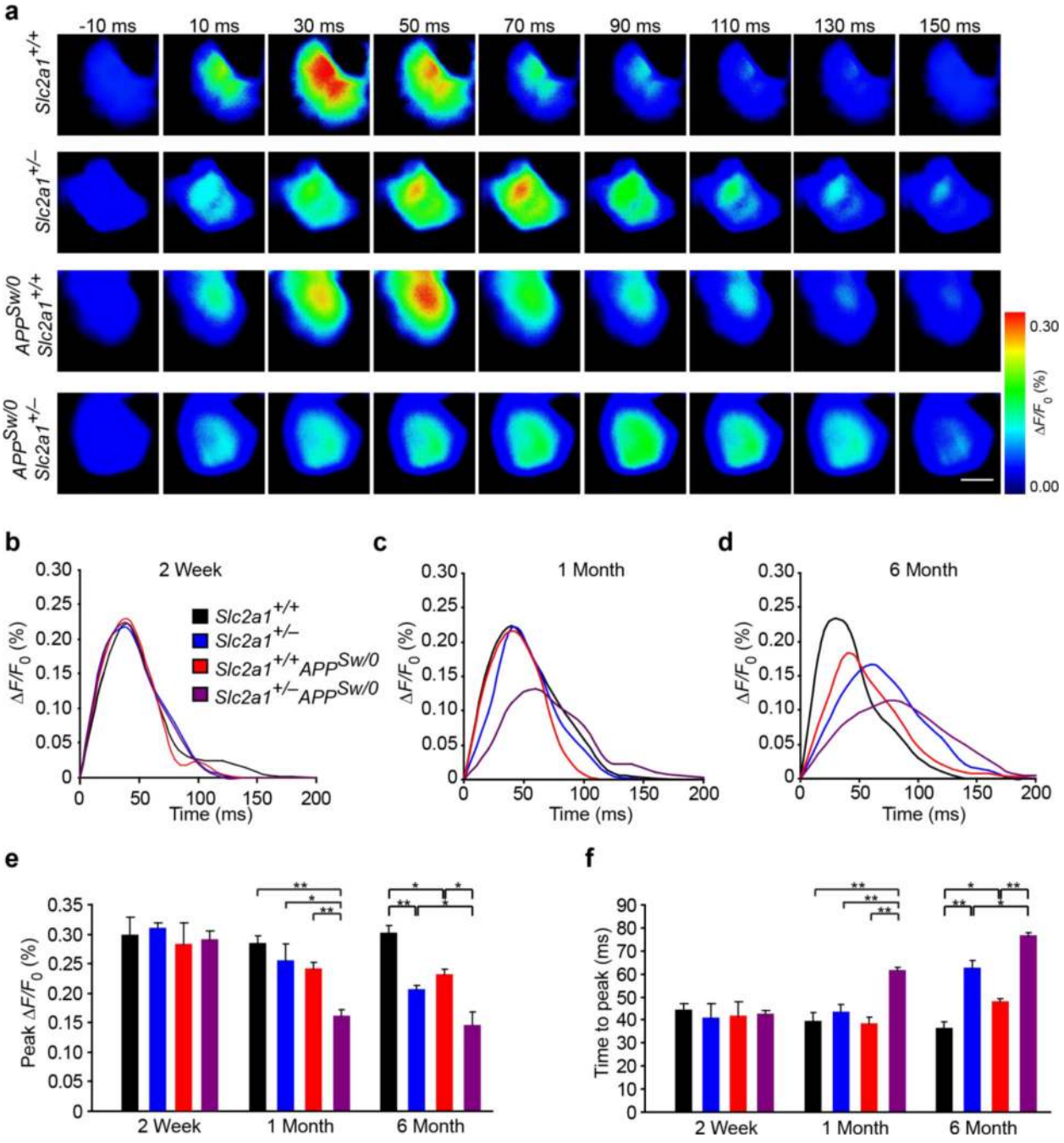

Figure 4. Neuronal dysfunction in GLUT1-deficient *APP*$^{Sw/0}$ mice

(**a**) Representative time-lapse-imaging analysis of voltage sensitive dye (VSD) signal response to hind-limb somatosensory cortex stimulation in 6-month-old *Slc2a1*$^{+/+}$, *Slc2a1*$^{+/-}$, *Slc2a1*$^{+/+}$*APP*$^{Sw/0}$ and *Slc2a1*$^{+/-}$*APP*$^{Sw/0}$ mice. Scale bar, 500 μm. (**b-d**) Quantitative time-lapse-imaging profile analysis of VSD response to hind-limb somatosensory cortex stimulation in 2-week-old (**b**), 1-month-old (**c**) and 6-month-old (**d**) *Slc2a1*$^{+/+}$, *Slc2a1*$^{+/-}$, *Slc2a1*$^{+/+}$*APP*$^{Sw/0}$ and *Slc2a1*$^{+/-}$*APP*$^{Sw/0}$ mice. $\Delta F/F_0$ indicates the percentage change in fluorescence from the baseline fluorescent signal following

stimulation. (**e-f**) Quantification of peak fluorescent VSD signal amplitude (**e**) and time-to-peak latency (**f**) in 2-week-old, 1-month-old and 6-month-old *Slc2a1*$^{+/+}$, *Slc2a1*$^{+/-}$, *Slc2a1*$^{+/+}$*APP*$^{Sw/0}$ and *Slc2a1*$^{+/-}$*APP*$^{Sw/0}$ mice. Mean ± SEM, n=3-4 mice per group; *p<0.05 or **p<0.01.

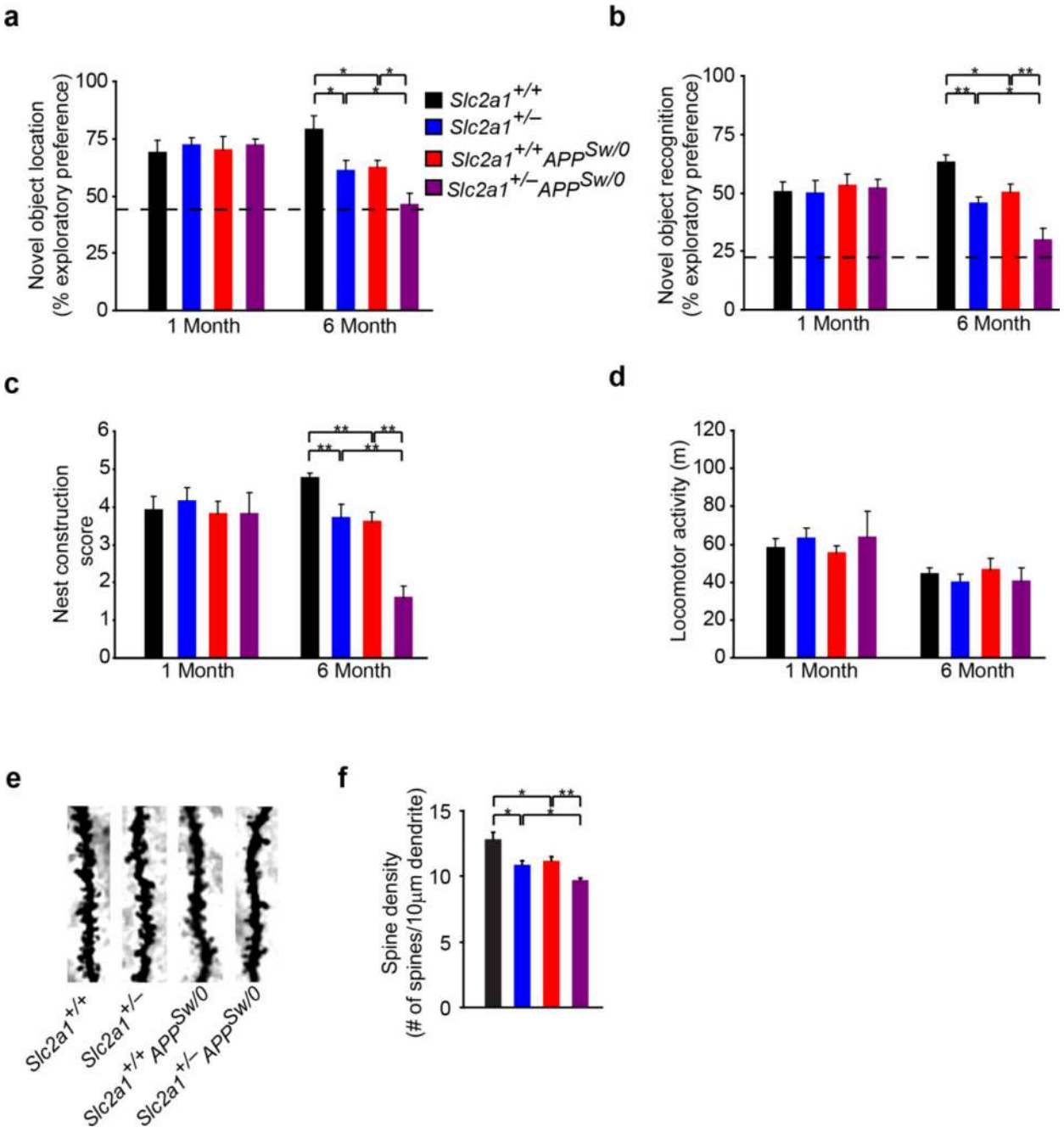

Figure 5. Accelerated cognitive impairment in GLUT1-deficient *APP*$^{Sw/0}$ mice

(**a-c**) Quantification of exploratory preference measuring hippocampal-dependent novel object location memory (**a**), novel object recognition memory (**b**), nest construction score (**c**) and mean locomotor activity (**d**) in 1- and 6-month-old *Slc2a1*$^{+/+}$, *Slc2a1*$^{+/-}$, *Slc2a1*$^{+/+}$*APP*$^{Sw/0}$ and *Slc2a1*$^{+/-}$*APP*$^{Sw/0}$ mice. Mean ± SEM, n=9-15 mice per group; *p<0.05 or **p<0.01. (**e**) Representative high-magnification bright-field microscopy microscopy analysis of Golgi-Cox staining showing dendritic spine density in the CA1 hippocampal region of 6-month-old *Slc2a1*$^{+/+}$, *Slc2a1*$^{+/-}$, *Slc2a1*$^{+/+}$*APP*$^{Sw/0}$ and *Slc2a1*$^{+/-}$*APP*$^{Sw/0}$ mice. (**f**) Quantification of dendritic spine density in 6-month-old

Slc2a1$^{+/+}$, *Slc2a1*$^{+/-}$, *Slc2a1*$^{+/+}$*APP*$^{Sw/0}$ and *Slc2a1*$^{+/-}$*APP*$^{Sw/0}$ mice. Mean ± SEM, n=3-5 mice per group; *p<0.05 or **p<0.01.

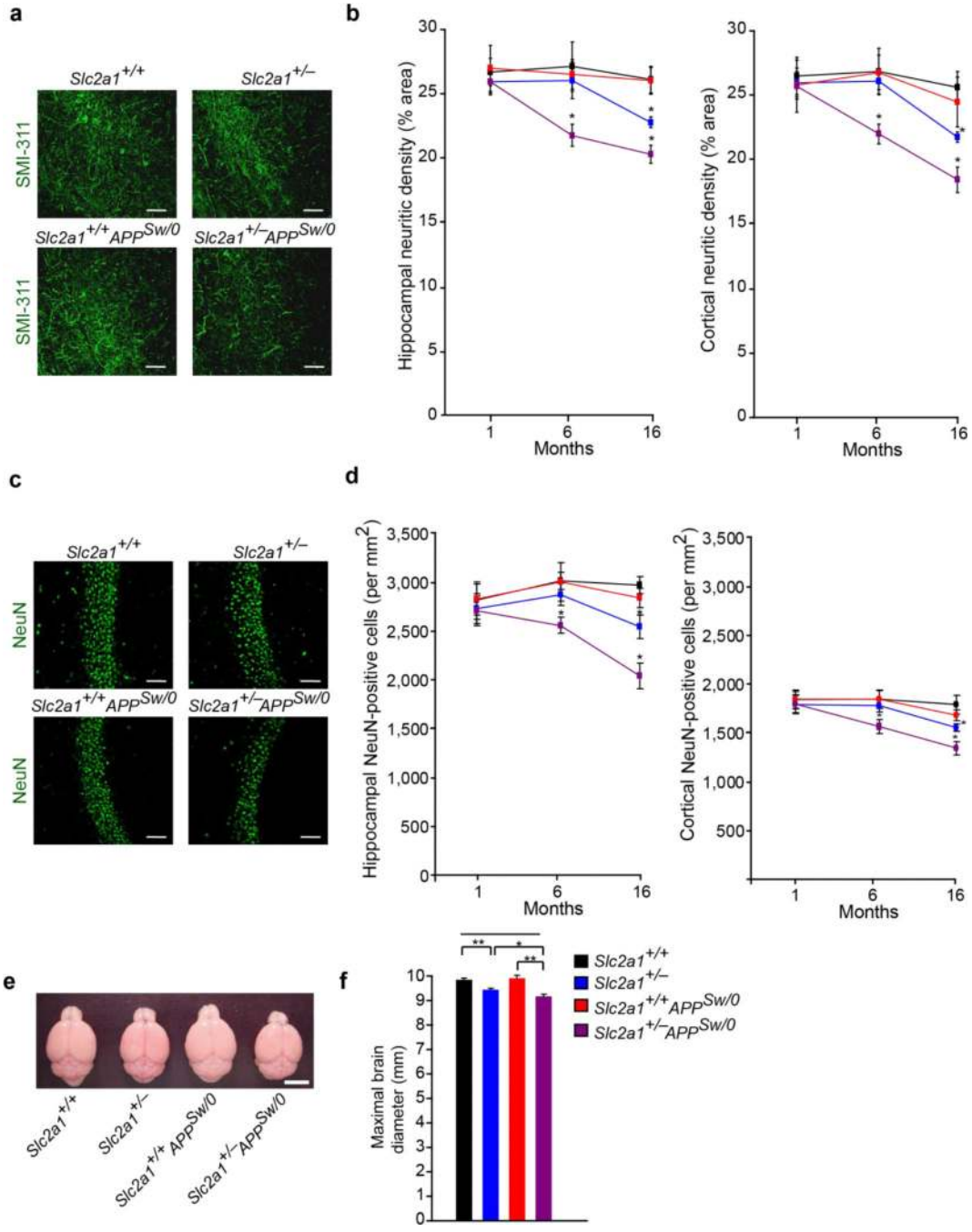

Figure 6. Accelerated neurodegenerative changes in GLUT1-deficient *APP$^{Sw/0}$* mice

(**a**) SMI-311 immunodetection showing neurites (green) in the CA1 hippocampal region of 16-month-old *Slc2a1$^{+/+}$*, *Slc2a1$^{+/-}$*, *Slc2a1$^{+/+}$APP$^{Sw/0}$* and *Slc2a1$^{+/-}$APP$^{Sw/0}$* mice. Scale bar, 50 μm. (**b**) Quantification of SMI-311-positive neuritic density in somatosensory cortex and CA1 hippocampal subfield in 1-, 6- and 16-month-old *Slc2a1$^{+/+}$*, *Slc2a1$^{+/-}$*, *Slc2a1$^{+/+}$APP$^{Sw/0}$* and *Slc2a1$^{+/-}$APP$^{Sw/0}$* mice. Scale bar, 50 μm. Mean ± SEM, n=3-4 mice per group; *p<0.05 or **p<0.01. (**c**) NeuN-positive neurons (green) in the CA1 hippocampal subfield of 16-month-old *Slc2a1$^{+/+}$*, *Slc2a1$^{+/-}$*, *Slc2a1$^{+/+}$APP$^{Sw/0}$* and

Slc2a1$^{+/-}$*APP*$^{Sw/0}$ mice. (**d**) Quantification of the number of NeuN-positive neurons in somatosensory cortex and CA1 hippocampal subfield in 1-, 6- and 16-month-old *Slc2a1*$^{+/+}$, *Slc2a1*$^{+/-}$, *Slc2a1*$^{+/+}$*APP*$^{Sw/0}$ and *Slc2a1*$^{+/-}$*APP*$^{Sw/0}$ mice. Mean ± SEM, n=3-6 mice per group; *p<0.05 or **p<0.01. (**e-f**) Representative low-magnification bright-field microscopy of mouse brains (**e**) and quantification of maximal brain diameter (**f**) in 6-month-old *Slc2a1*$^{+/+}$, *Slc2a1*$^{+/-}$, *Slc2a1*$^{+/+}$*APP*$^{Sw/0}$ and *Slc2a1*$^{+/-}$*APP*$^{Sw/0}$ mice. Scale bar, 5 mm. Mean ± SEM, n=5-6 mice per group; *p<0.05 or **p<0.01.

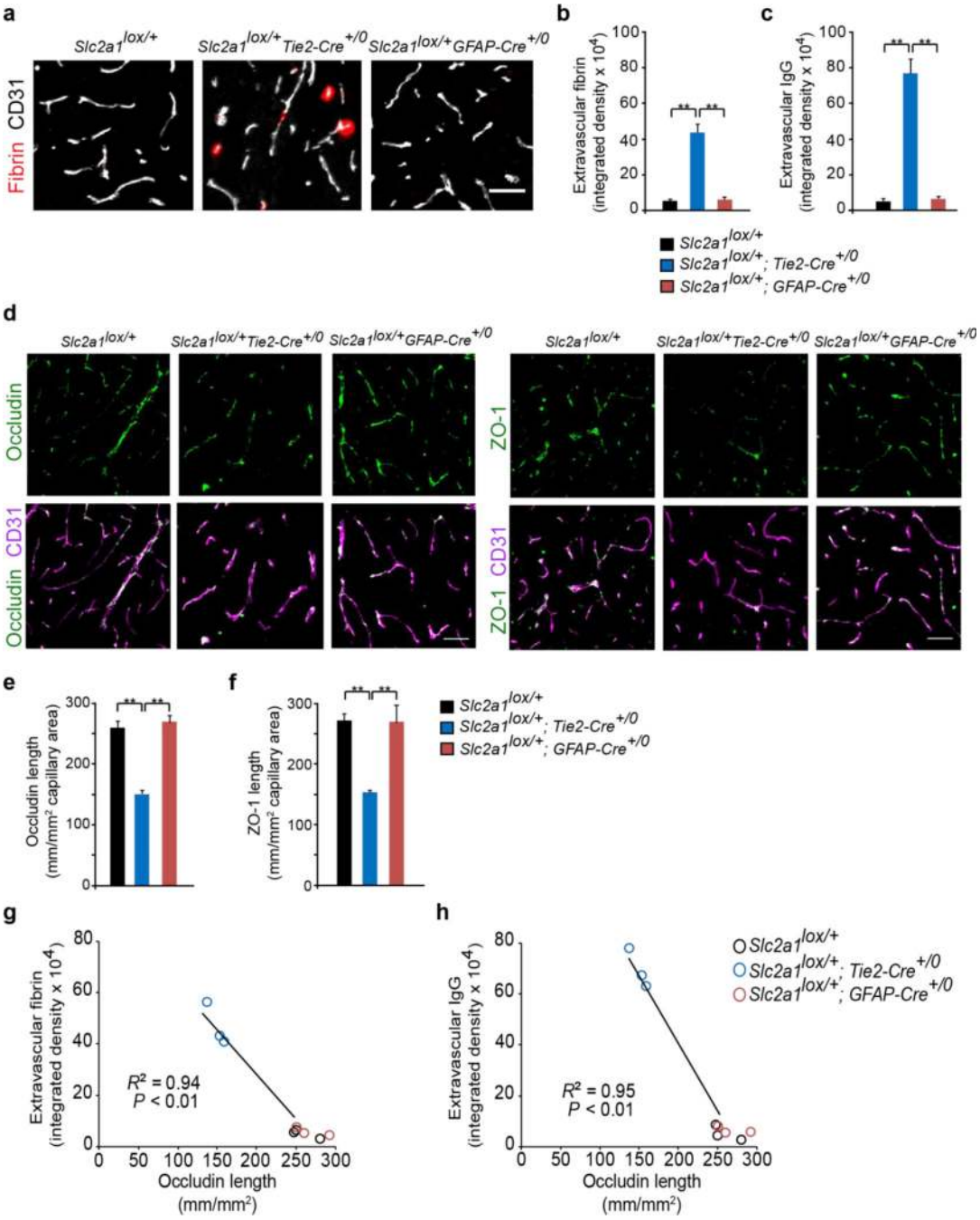

Figure 7. GLUT1 deficiency in endothelial cells (*Slc2a1$^{lox/+}$Tie2-Cre$^{+/0}$* mice), but not astrocytes (*Slc2a1$^{lox/+}$GFAP-Cre$^{+/0}$* mice) leads to early BBB breakdown

(**a**) Representative confocal microscopy analysis of plasma-derived fibrin (red) and CD31-positive capillaries (white) in 2-week-old *Slc2a1$^{lox/+}$*, *Slc2a1$^{lox/+}$Tie2-Cre$^{+/0}$*, *Slc2a1$^{lox/+}$GFAP-Cre$^{+/0}$* mice. Scale bar, 25 μm. (**b-c**) Quantification of extravascular fibrin (**b**) and IgG (**c**) positive deposits in 2-week old *Slc2a1$^{lox/+}$*, *Slc2a1$^{lox/+}$Tie2-Cre$^{+/0}$*, *Slc2a1$^{lox/+}$GFAP-Cre$^{+/0}$* mice. Mean ± SEM, n=3-5 mice per group; *p<0.05 or **p<0.01. (**d**) Representative confocal microscopy analysis of the tight junction proteins occludin or

zonula occludens-1 (ZO-1) (green) and CD31-positive capillary profiles. (**e-f**) Quantification of endothelial occludin (**e**) and ZO-1 (**f**) tight junctional length in the microvessels in 2-week-old *Slc2a1*$^{lox/+}$, *Slc2a1*$^{lox/+}$*Tie2-Cre*$^{+/0}$, *Slc2a1*$^{lox/+}$*GFAP-Cre*$^{+/0}$ mice. Scale bar, 25 μm. Mean ± SEM, n=3-5 mice per group; *p<0.05 or **p<0.01. (**g-h**) Negative correlation between extracellular fibrin (**g**) or IgG deposits (**h**) and decreased occludin length in the microvessels in 2-week-old *Slc2a1*$^{lox/+}$, *Slc2a1*$^{lox/+}$*Tie2-Cre*$^{+/0}$, *Slc2a1*$^{lox/+}$*GFAP-Cre*$^{+/0}$ mice.